Master of Science

Pressure barrier of water using superhydrophobic surface and its application for a pressure relief valve

The Graduate School

of the University of Ulsan

Department of Mechanical Engineering

Eunsik Kim

Pressure barrier of water using superhydrophobic surface and its application for a pressure relief valve

Supervisor: Professor Doo Man Chun

A Thesis

Submitted to

the Graduate School of the University of Ulsan

In partial Fulfillment of the Requirements

for the Degree of

Master of Science

by

Eunsik Kim

Department of Mechanical Engineering

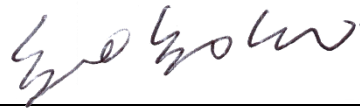University of Ulsan, Republic of Korea

December 2020

Pressure barrier of water using superhydrophobic surface

and its application for a pressure relief valve

This certifies that the master's thesis

of Eunsik Kim is approved.

_____
Committee Chair Prof. Bo Hung Kim

_____
Committee Member Prof. Kyoungsik Chang

_____
Committee Member Prof. Doo-Man Chun

Department of Mechanical Engineering

University of Ulsan, Korea

November 2020

CONTENTS

ABSTRACT

In fluid systems, pressure relief devices are essential and there are various types of mechanical pressure relief devices. However, this mechanical pressure relief device involves inevitable problems such as corrosion and moving errors. in this research, by using varies types of hole on superhydrophobic surfaces that was fabricated with silica nanoparticles and PDMS, effects of pressure barrier and releasing behavior under hydraulic pressure were described. the pressure barrier induced by unique wetting mode on hydrophobic/superhydrophobic surfaces and the infiltration pressure is according to classical Young-Laplace equation. by using single hole, multiple holes and porous medium, an effect of number of holes to the pressure barrier was identified. Furthermore, through the computational fluid dynamics (CFD) simulations, the infiltration pressure verification and pressure releasing behavior on the pressure barrier were analyzed. the results can be applied to the novel type of pressure relief device using the pressure barrier.

LIST OF FIGURES

LIST OF TABLES

1. INTRODUCTION

Pressure relief devices are essential to maintain operational condition or prevent breakage in a fluidic system. Typical pressure relief devices operate on mechanical basis. As shown in Figure 1, it is mostly the installation of separate devices using elastic structures like a spring to open and close valves in the fluid system. Therefore, these types of mechanical devices inevitably involve problems such as corrosion of elements or operational moving errors. Because of this, various non-mechanical types of pressure relief devices were described for a decade. Many studies have been investigated on the form of non-mechanical pressure valves using capillary forces in micro channels.[1–5] However, this type of valve requires multiple channels and has limitations in machining difficulty and material wetting properties. For this reason, research is needed to enhance wettability and apply.
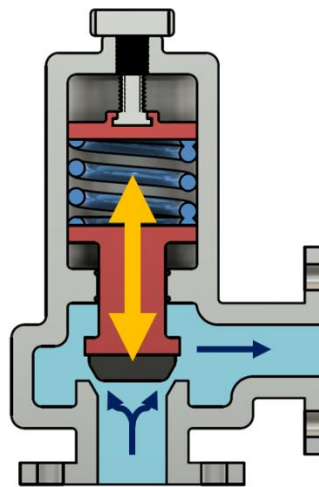
Figure 1. Schematic image of mechanial pressure relief valve.

A superhydrophobic surface have been attracting because of the unique properties of superhydrophobic surfaces. The superhydrophobic surface is defined as having a static water droplet contact angle (CA) greater than 150° and a sliding angle (SA) less than 10°. Wettability is the fundamental property of solid surface. The surface energy of dry solid along with Young's relation, is less than surface energy of wet solid, so the liquid on the surface is formed unique wetting mode.[6] Because of this, surface tension on a hydrophobic/superhydrophobic surface oppose to distortion and spread. Therefore, a pressure barrier is formed that prevents the water from infiltrating into empty spaces on superhydrophobic surfaces.[7] This pressure barrier that supports the hydraulic pressure on the surface is required studies the behavior of the critical load pressure and pressure of the barrier. The effect of this pressure barrier can improve the performance of non-mechanical pressure relief valves or be applicable to other applications such as air-vent channel.

In general, the superhydrophobic property is caused by rough surfaces and low surface energy. In this research, a simple and inexpensive dip-coating method is presented to fabricate superhydrophobic coating on aluminum surfaces using polydimethylsiloxane (PDMS) and silica nanoparticles.[8] Aluminum (Al) and its alloys are important materials. Because of its good ductility, low specific weight, and excellent electrical conductivity. PDMS and silica nanoparticles are applied by the dip-coating method, simultaneously including ordered roughness and low surface energy.[9][10] PDMS is a well-known material with low surface energy. Because of its hydrophobic property and intrinsic deformability, PDMS can be made into superhydrophobic. And Silica particles can improve the nano-microstructures. Such structures can be functionalized superhydrophobic surfaces.

Accordingly, in this research the behavior of pressure barrier on superhydrophobic surfaces were investigated by experimental results and the capillary theoretical approach. In addition, the pressure relief at the pressure barrier and its phenomena were simulated and compared through the numerical analysis method. The result of pressure barrier effect can be applied to construct a pressure relief device that is non- mechanical pressure relief device.

2. EXPERIMENTAL DETAILS

2.1. Superhydrophobic surfaces preparation
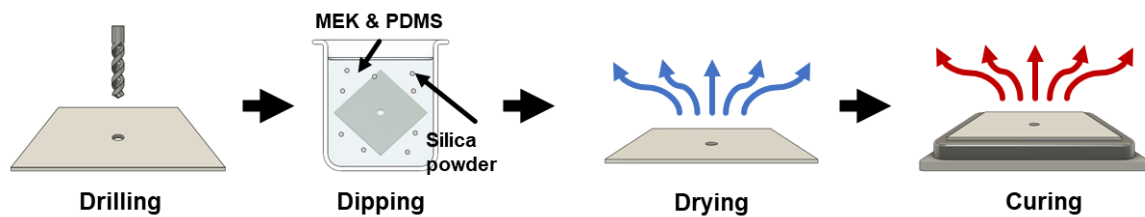
Figure 2. Shematic of dip-coating process

Dip-coating process carried out to change the surface wettability of samples. Plates (30x30x1mm3) of high machinability and widely used Al alloy (Al6061) were used in this research. Before processing, all plates were drilled a hole at the center by milling brill (Dremel 3000, Dremel workstation 220, Dremel, USA). The high-speed steel drill bits were used for milling (HSS mini drill bit, HSS, FALCON, Korea). The size of the hole is divided 6 types, $0.5\,mm$, $0.6\,mm$, $0.7\,mm$, $0.8\,mm$, $0.9\,mm$ and $1.2\,mm$. Furthermore, the largest hole size ($1.2\,mm$) was selected because the infiltration pressure had a convergent value as the size of the hole grew.

Hydrophobic PDMS (Polydimethyl siloxane, DOW CORNING, USA), silica nanoparticles (SiO2, Konasil, OCI Co Ltd, Korea) and MEK (2-Butanone, 99.7%, SAMCHUN, Korea) were used for dip-coating to create a low surface energy and additional nano-microscale structure on the surface of the Al sheet. The compositions of MEK, silica nanoparticles and PDMS were 94wt%, 5wt% and 1wt% respectively. The dip-coating

process was carried out the 20 sec, and then dip-coated sample were dried at room temperature for 1 h and heated at 150℃ for 15 min, as shown Figure 2.

2.2. Surface analysis

The CA and the SA were measured using a contact angle meter (Smart drop, Femtolab Co. Ltd., Korea). For CA and SA measurements, three positions were used for each dip-coated sample, and the volume of the water droplets was 11 μl. For SA, a tilting speed of 0.8°/s was used. In addition, the type of wettability, i.e., the Wenzel state (full wetting) or the Cassie-Baxter state (partial wetting), was observed from the optical images. Dimension of the hole was determined by the circle made with the three points of the surface on the edge of the hole, which based on height profiles and optical images of the confocal microscope (VK-X200 series, Keyence, Japan) as shown like Figure 3. The surface morphology was observed by means of field emission scanning electron microscopy (FE-SEM, JSM-7600, Jeol Com., Japan)
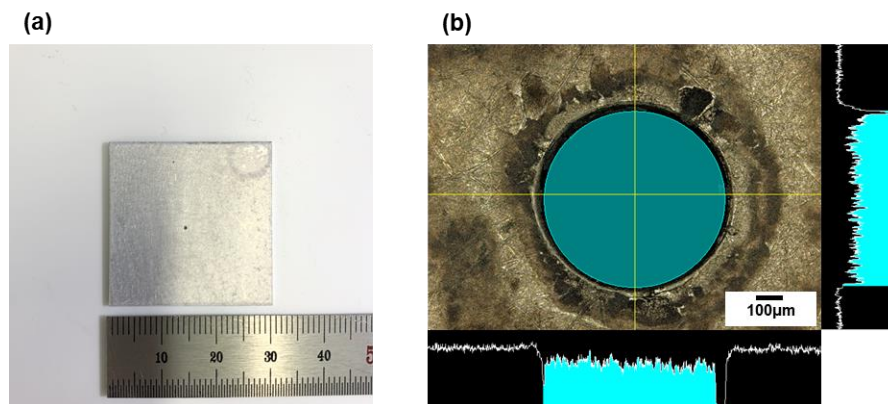
Figure 3. (a) image of dip-coated Al plate, (b) confocal image and height profile of dip-coated hole.

2.3. Evaluation of pressure barrier

The experimental equipment was constructed as shown in Figure 4 (a). The cylindrical quartz tube (Φ=22 mm, t=1.5 mm) were used and clamped dip-coated plate by sealing with silicon rings. The water was supplied gently along the inner wall of the cylinder using a syringe to minimize disturbances so that the surface of water would rise without oscillation. At the time of the leakage of water initiated through the hole, the supplying water was stopped. After finished the leakage, water was fed against as in previous. In this study, pressure barrier induced by superhydrophobicity was indicated by pressure head. The measurement was taken recording heights that are start point of water infiltrating to hole (h_I) and end point of releasing (h_E), as shown like Figure 4 (b). The h_I and h_E were measured five times at once.
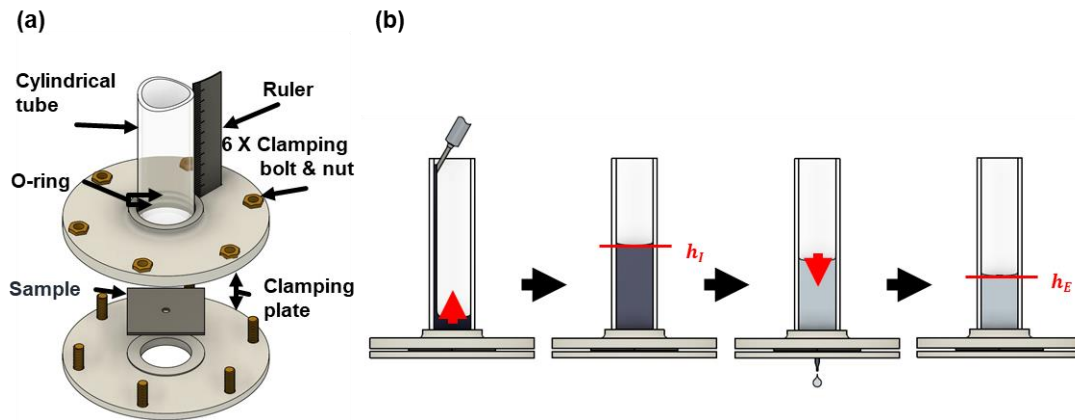
Figure 4. Schematic images of (a) exprerimental equipment and (b) evaluation of pressure barrier.

3. RESULTS AND DISCUSSION

3.1. Wettability and surface morphology

The variety paper of superhydrophobic surfaces represented low surface energy materials can treat to superhydrophobic surfaces with surface roughness in microscale and nanoscale. The dip-coated Al substrates had microscale structures, as shown in Figure 5 (A). The microscale structures predominantly covered on the surface. Silica nanoparticles-PDMS composites were made by mixing a polymer binder with silica particles ranging from 7 nm to 40 nm in diameter. As these silica nanoparticles created the nanoscale roughness on the microscale structure, the coated Al substrate had a hierarchical structure of the microscale and nanoscale, as shown like Figure 5 (D). By having the structure of these two scales, such as lotus leaves, the hydrophobic property of the surface of the coated substrate is enhanced.[11][12] This coated Al plate showed 168.7° of the static contact angle and 7.3° of the sliding angle, as shown in Figure 6.
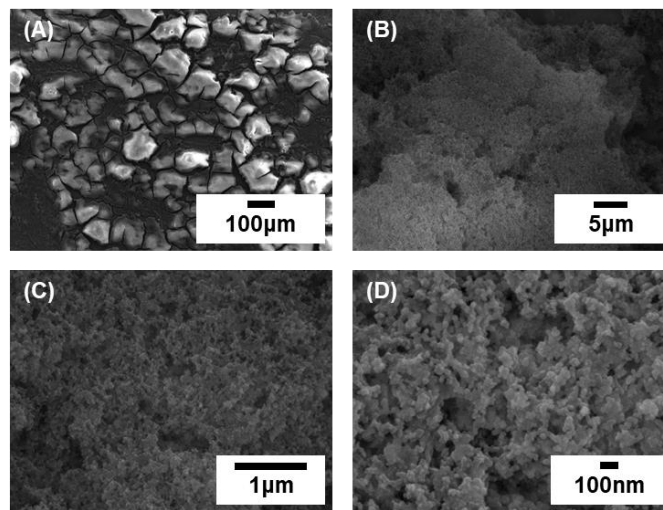
Figure 5. FE-SEM images of dip-coated Al plate.
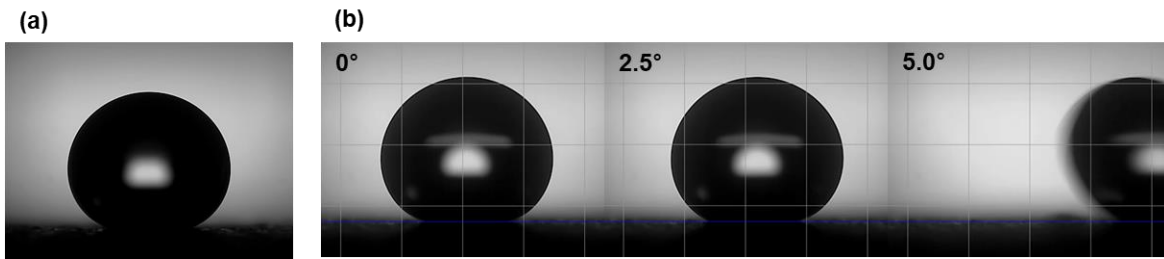
Figure 6. (a) image of CA, (b) images of SA.

3.2. Pressure barrier with single hole

The infiltration and released pressures were determined by heights of starting of leakage and finishing of releasing. When the pressure of supplied water in the cylinder reached the critical value, the pressure barrier at the edge of hole was broken and pressure released through the hole. The critical pressure, which is the infiltration pressure, for sustain a hydraulic pressure was shown as following Figure 7. After releasing the pressure caused by exceeding the infiltration pressure to the barrier, the flow of discharged water through the hole abruptly stopped as the flow gradually slowed and changed from continuous flow to discontinuous flow, as shown like Figure 8. The discharged water could be separated from the end of the hole by the gravity force of the water droplet was over the force of surface tension.[13] But when the flow wasn't enough to create the droplet to detach from the edge, the pressure releasing stopped. Upon completion of pressure releasing, the remaining water in the hole was pushed back to the upper side of the hole by surface tension and formed the pressure barrier as before. thus, applying additional pressure to the stable condition after

8

relief, it remained stable by the pressure barrier until the infiltration pressure. This pressure releasing mechanism was appeared when the direction of the hole equal with the gravity. Therefore, different direction of the hole axis can show the degree of pressure released. In addition, experiments, as shown in Figure 9, where hydrophilic structures were installed near the end of the hole in such a way that the discharged water droplets could spontaneously separate, continued to release until the pressure was fully released.
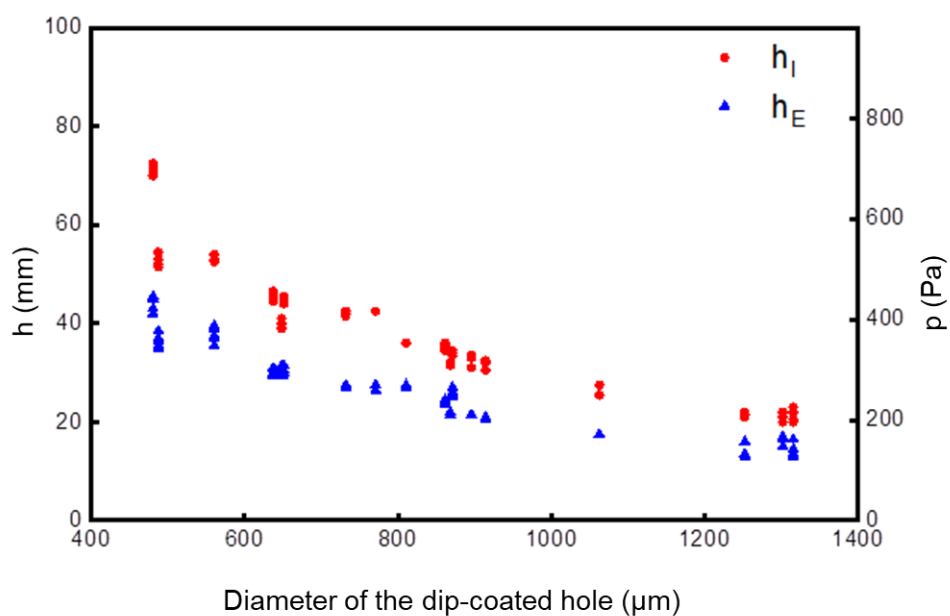
Figure 7. Pressure barrier with single hole.
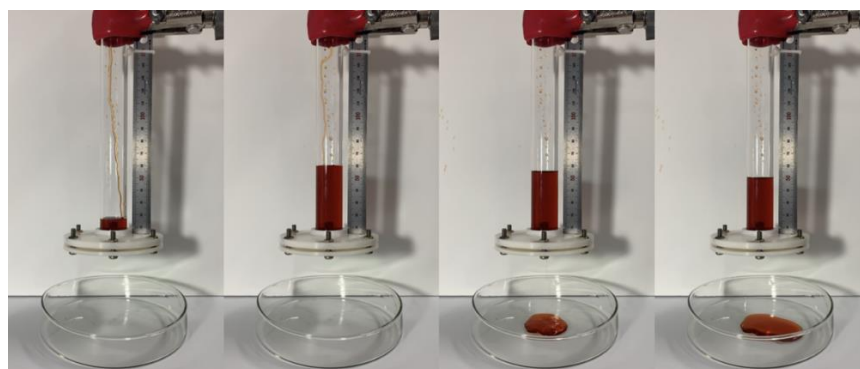
Figure 8. Demonstration of pressure relief at the pressure barrier on superhydrophobic surfaces

9
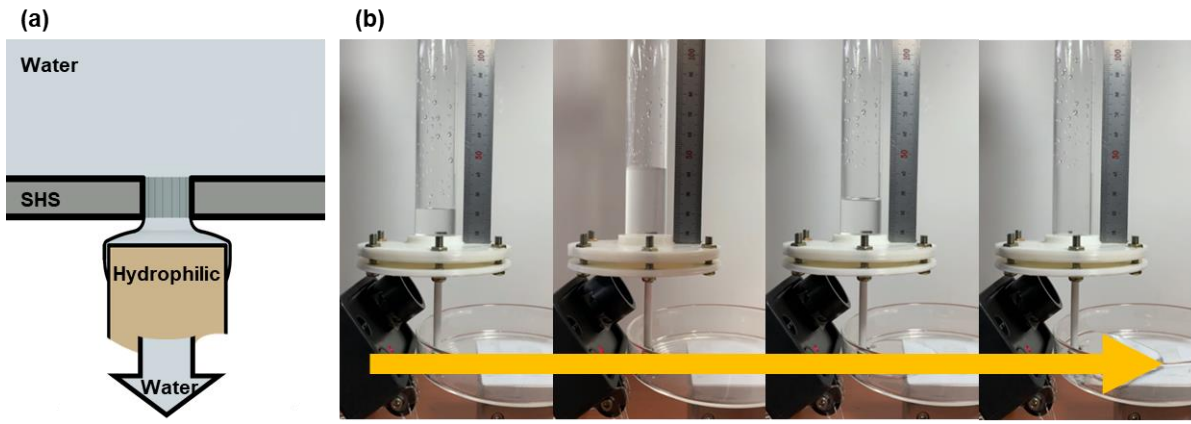
Figure 9. (a) schematic image of removing gravity term for separating droplet,
(b) demonstration of removing gravity term for separating droplet.

3.3. Young-Laplace equation
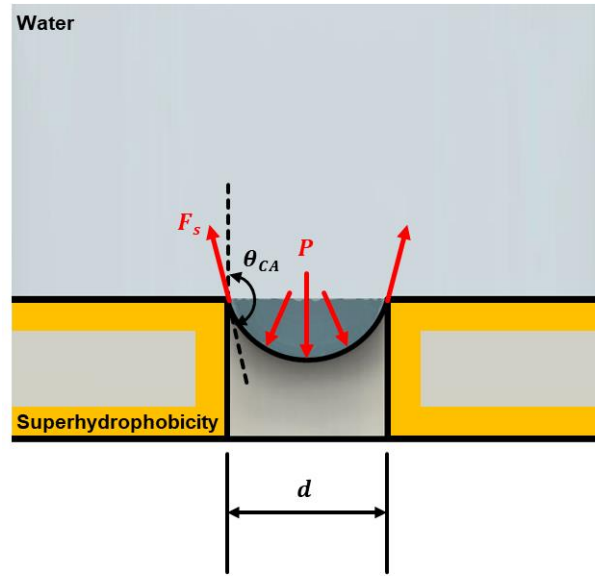
Figure 10. schematic of Young-Laplace equation.

According to hydrostatic equilibrium, the pressure barrier is formed by surface tension between the superhydrophobic surfaces and the liquid. The following Figure 10. is a schematic image of the pressure barrier forming in a circular hole on a superhydrophobic surface and the forces acting on the barrier. At microscale, Young-Laplace equation is used to define the equilibrium of liquid surface.[14]

$$\Delta p = \gamma \left(\frac{1}{R_1} + \frac{1}{R_2} \right) \tag{1}$$

where $\Delta p, \gamma$ are the pressure difference across the liquid surface, the liquid surface tension, R_1 and R_2 are the principal radii of surface curvature. In addition, in a sufficiently narrow

cylindrical hole (with radius a), the liquid surface will be a portion of spherical surface (with radius a) and R is related to a by the contact angle θ ($R = a/cos\theta_{CA}$). Thus, theoretical infiltration pressure of the pressure barrier is computed by modified Young-Laplace equation, which is given as:

$$\Delta p = \frac{2\gamma \cdot cos\theta_{CA}}{a} \qquad (2)$$

Therefore, expressing the infiltration pressure at the barrier as pressure head is given by:

$$h = -\frac{4\gamma \cdot cos\theta_{CA}}{\rho g d} \qquad (3)$$

Where ρ, g, d are density of liquid, acceleration of gravity and diameter of the hole. In this research, the surface tension was set at $0.072\ N/m$ [15]. As shown in Figure 11, the infiltration pressure obtained through the experiment was shown similar to the theoretical infiltration pressure according to Young-Laplace equation, and the trend shown by the experimental results was similar. The infiltration pressure at the barriers on superhydrophobicity holes are determined by the hole size, indicating that this can be estimated through Young Laplace equation. The hole size and infiltration pressure are in inverse proportion, which means that greater pressure is required for flow to pass through the hole in the smaller hole. Moreover, for the effect of pressure barrier, surface have to show hydrophobic or superhydrophobic surfaces which have a contact angle of more than 90°.
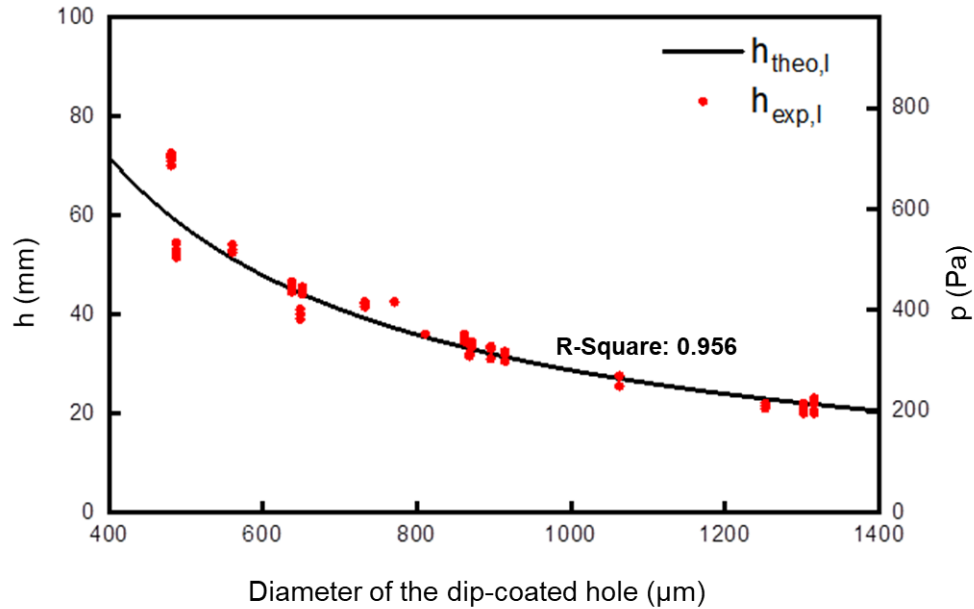
Figure 11. Experimatal infiltration pressure at a pressure barrier
with Theoretical infiltration pressure according to Young-Laplace equation.

3.4. Computational fluid dynamics simulation

Additionally, in this study numerical analyses were made through computational fluid dynamics (CFD) to analyze the formation of pressure barriers on superhydrophobic surfaces and the behavior of pressure relief mechanisms. In this study, the governing equations are the incompressible unsteady Navier-Stokes equations for three-dimensional laminar flow. The volume fraction α in each cell in the computational domain is between 0 and 1. This quantity is defined as the percentage of water phase volume contained inside the computational cell relative to the cell total volume. The continuity and momentum equations for laminar, incompressible, Newtonian and isothermal flow are as follows:

13

$$\nabla V = 0 \tag{4}$$

$$\frac{\partial \rho \vec{V}}{\partial t} + \nabla(\rho \vec{V} \vec{V}) = -\nabla P + \nabla\left[\mu\left(\nabla \vec{V} + \nabla^T \vec{V}\right)\right] + \vec{F}_{vol} \tag{5}$$

Where, V, P, ρ, t, F_{vol} and μ are the velocity of mixture, pressure, time, density, volumetric force and viscosity, respectively. The analysis was carried out using the volume of fluid (VOF), which allowed continuous tracking of laminar models and surfaces. the density of the mixture is updated by using the volume fraction, which is given by:

$$\rho = \alpha \rho_w + (1 - \alpha)\rho_a \tag{6}$$

where ρ_a and ρ_w are the air and water densities. The time step was set to 0.01 sec and the modeling of the wall was done using the continuum surface force (CSF) model.[17][18] The volumetric force due to the surface tension at the interface is given by:

$$F_{vol} = 2\sigma \frac{\rho \kappa \nabla \alpha}{\rho_a + \rho_w} \tag{7}$$

where, σ and κ are the air/liquid tension force and the interface curvature. The interface curvature k is given by:

$$\kappa = \nabla \cdot \hat{n} \qquad\qquad (8)$$

Where $\hat{n} = n/|n|$ is the unit normal vector to the interface.

The CFD simulation was performed using ANSYS Fluent 18.2. The numerical analysis was conducted on, 560 μm, 650 μm, 730 μm, 810 μm and 900 μm, total five cases using the same values as the size of the holes used in the experiment. The height of the capillary tube inside the cylinder was set at 70 mm, the diameter of the capillary tube is 18.8 mm, and the height of the outlet of water escaping under the dip-coated plate was set at 5 mm, as shown in Table 1. The grid was created by structured mesh, and the grid size was set at 0.5 mm for the ± 10 mm section of the release pressure point measured in the experiment, and the height of the first grid from the wall was set at 0.01 mm, as shown in Figure 12. The CA at the quartz cylinder tube was set at 26.8°[16] and the CA at the superhydrophobic surface was set at 168.7°, and the surface tension coefficient between water and air was set at 0.072 N/m, as shown in Table2.
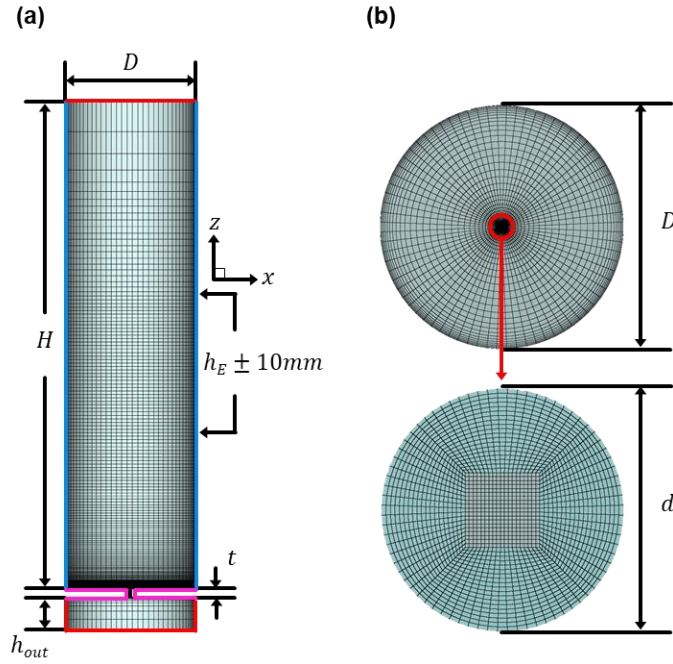
Figure 12. The structured mesh (tube, hole) with wetting properties of wall.

	Unit [mm]	
D	Tube diameter	18.8
d	Hole diameter	...
t	Sample thickness	1
H	Tube height	70
h	Outlet	5

Table 1.Dimension of structured mesh (tube, hole).

Boundary Condition
Pressure Outlet
Wall (Tube $\theta_{CA} = 26.8°$)
Wall (SHS $\theta_{CA} = 168.7°$)

Table 2. Wetting properties of structured wall surfaces.

Analytical results of h_E was determined by using the average value of 99% and 1% of the volume fraction of water because accurately track the water surface inside the quartz cylinder was difficult.

Similar with the theoretical study, numerical results also showed that pressure barriers were formed by surface tension on the superhydrophobic surfaces and this barrier sustained stably below the infiltration pressure according to Young-Laplace equation, as shown in Figure 13 (a). But, when over the pressure was applied for the first time, it continued to occur releasing until the pressure relief was terminated. For the progress of pressure releasing, unlike experiments in which water flows down the inner wall of the cylinder, the analysis was conducted at a height 10 mm higher than the measured height of the infiltration pressure in the experiment. Because the water is pulled by the surface tension of the cylinder wall and the water level is lowered by formed meniscus. At the same time as the analysis progressed, continuous pressure relief from the hole followed by in the cylinder as in the experiment, showing that the water surfaces lowered with making meniscus. As shown in the Figure 13 (b), the pressure releasing was terminated when the flow in the hole decreased at the initiating of relief and the separation of the discharged water droplet became unstable and the gravity force to the droplet smaller than the tension of the water. This discharge pressure showed results same as the experiment as shown in Figure 14. And CFD analysis showed that residual water inside the hole retreat at the moment the pressure releasing was completed, creating a pressure barrier on the top of hole. This retraction occurred when the surface tension caused by the superhydrophobic of the hole pushed back the residual water. CFD results showed that

17

pressure releasing behavior at the pressure barrier that formed on superhydrophobic holes can be simulated, and the end of pressure releasing is also predictable.
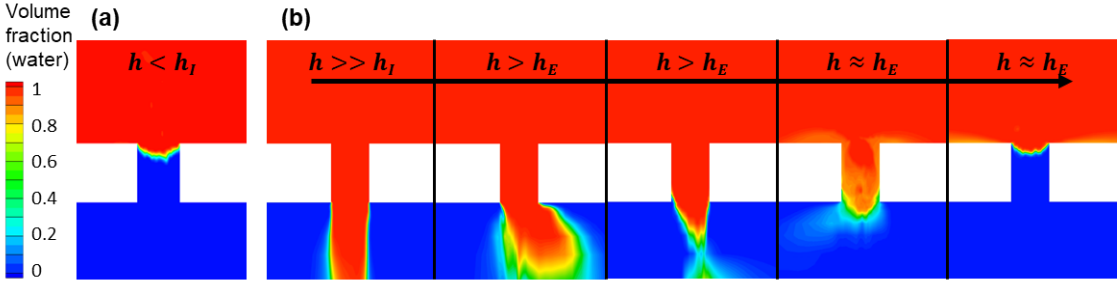

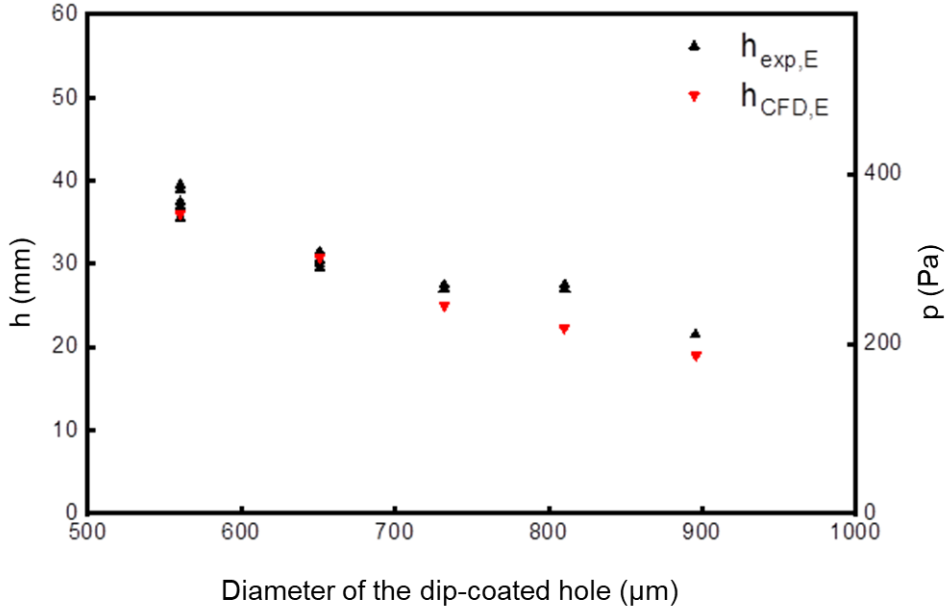Figure 13. Volume fraction contour at the superhydrophobicity hole.

Figure 14. End of pressure releasing with CFD rsults.
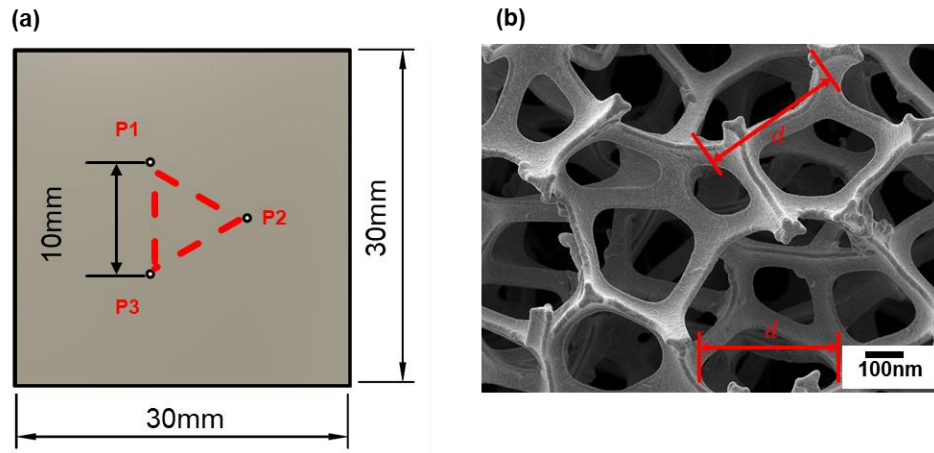
3.5. Pressure barrier with multiple holes

Figure 15. (a) schematic image of a dip-coated Al plate with three holes, (b) FE-SEM image of Ni foam sheet.

In this research, a surface with three holes and porous structure were used to study the effects of pressure barriers with multiple holes. The surface with three holes was made in a form with a sufficient distance between the holes to minimize the impact of possible interference by machining, as shown like Figure 15 (a). we prepared the dip-coated Al plate with three holes which were made by same size of drill beat. Each hole size was determined by observing confocal microscope as same single hole. the infiltration pressure and positions of releasing hole are summarized in Table 3. When pressure reached to infiltration pressure at the largest hole on surfaces, pressure releasing was started immediately. At loaded lower than the infiltration pressures of the other two holes, the pressure barrier at the holes was stable and pressure relief was progressed only in the largest holes on the surface. The infiltration pressure on a surface with multiple holes was determined according to the largest hole on the surface. In addition, the experimental results were within 3% errors from that of

Young-Laplace equation. When the water was supplying consistently even the pressure releasing had started at the largest hole, the pressure released step by step in order of large holes, as shown in Figure 16. The discharged water emitted in the same aspect as in the single hole on the superhydrophobic surface the flow gradually slowed and the discharge is terminated momentarily. The pressure releasing stopped first from the smallest hole and the pressure releasing was completed at the largest hole on the surface.

Sample No.	Position	d [μm]	Leak position	h_l [mm]	h_{Theo} [mm]	error(%)
1	P1	658				
	P2	625		43.4 ± 1.1	43.0	0.91
	P3	666	P3			
2	P1	662				
	P2	678	P2	41.5 ± 2.0	42.6	2.48
	P3	666				
3	P1	673				
	P2	676	P2	43.4 ± 0.5	42.5	2.01
	P3	670				
4	P1	659				
	P2	672	P2	43.2 ± 1.7	43.4	0.44
	P3	672	P3			
5	P1	683	P1			
	P2	663		43.5 ± 1.5	42.2	2.96
	P3	672				

Table 3. Pressure barrier with multiple holes (3 holes).

Figure 16. Demonstration of pressure relief by step depending on the hole size.

Additionally, Ni foam sheet (purity, 99.5%, 110 PPI, density of 350 g m2, and 1.6 mm thickness, Invisible, Inc.) was used for study about pressure barrier on porous structure. The dip-coating process was carried out same with the Al plates, but for permeating the dip-coating solution to the porous medium, the dipping process was taken for 2 min. Hole sizes of dip-coated Ni foam sheets was determined by SEM image, as shown like Figure 15 (b). As shown in the image, the hole had a tilted shape, so the longest length of the cross section was assumed to be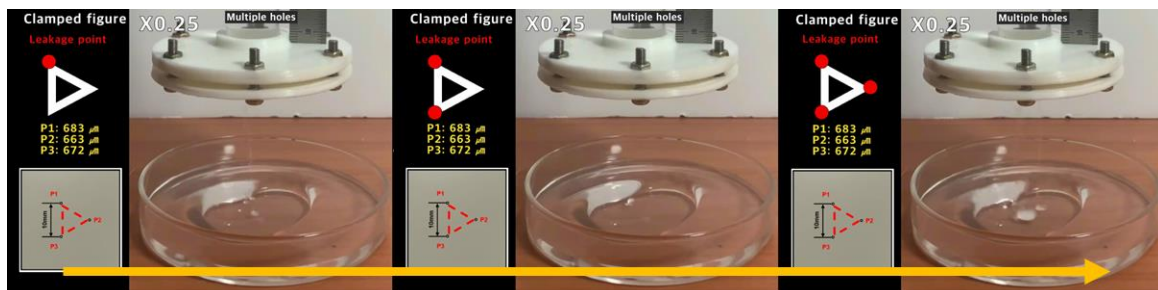 the diameter. When water was supplied to the cylinder equipped with dip-coated Ni foam sheet, the pressure barrier was formed at each hole of the porous structure as in single hole. The pressure barrier formed at each of these holes began to release the hydraulic pressure when pressure reached to infiltration pressure according to Young-Laplace equation within 5% errors, as shown in Table 4. The pressure releasing also showed the same process, but the released pressure progressed more, and the releasing completed at a lower value than the release pressure in the single hole. It was caused by the structural characteristics of porous medium. When water was re-fed after the initial pressure release was completed, the infiltration pressure was significantly lower than the initial infiltration pressure value. The water passing through the porous medium during the relief of pressure exceeding the infiltration pressure at the initially formed pressure barrier and was remained after the release. because of residual water, the water easily made a channel in the medium and the pressure barrier was shown weaker than the initial infiltration pressure barrier according on the porous size. In addition, that led to more pressure releasing than the initial pressure releasing process, unlike for single and three holes. However, if the dip-coated Ni

21

foam sheet was dried and the residual water was completely removed, it again showed the same value as the initial infiltration pressure determined according to the porous size.

Sample No.	h_I [mm]	h_E [mm]	h_{Theo} [mm]	error [%]
1	78.0	42.0		
2	71.5	38.0		
3	75.5	49.5	78.4	3.6 ± 3.3
4	77.5	55.5		
5	81.5	47.0		

Table 4. Pressure barrier with multiple holes (Ni porous medium).

The pressure barrier formed with multiple holes, as shown in Figure 17, is determined by Young-Laplace equation, the same as when the holes are a single hole. However, during the pressure releasing process, such as the porous structure, the discharged flow rate from each hole was combined at the end, making it easier for the droplets to separate than in a single hole, resulting in a greater degree of pressure discharge.
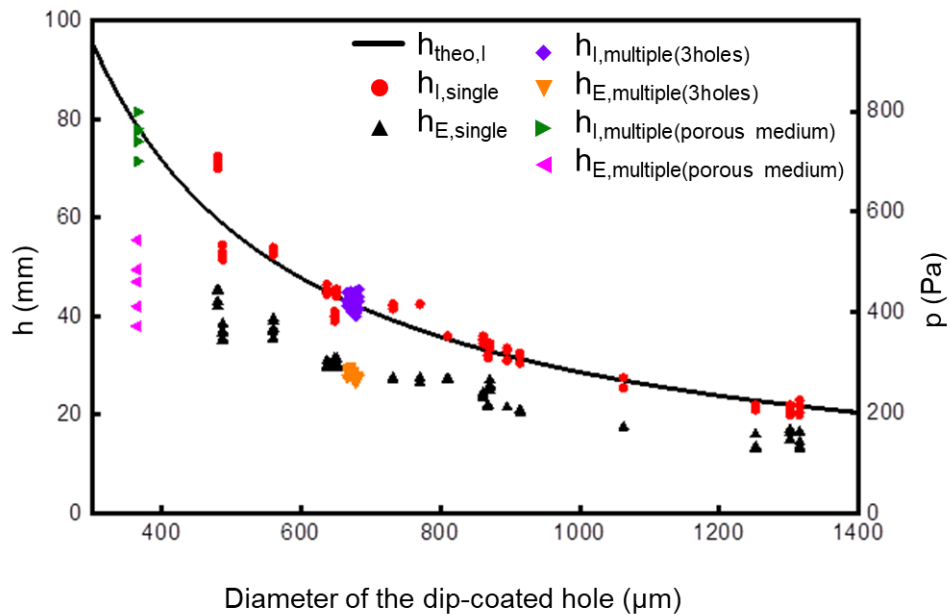

Figure 17. Pressure barrier with multiple holes.

3.6. Design issue for a pressure relief valve

As with the previous results, a hydrophobicity/superhydrophobicity hole forms a pressure barrier in the interface with water under pressure, and this pressure barrier showed that the infiltration pressure was determined by the size of the hole. It is possible to construct a fluid system with the pressure relief hole of a determined size based on the required pressure of design. As shown in Figure 18(a) and (b), when water was supplied to a channel of the fluid system with the uncoated Al plate is installed, the water overflowed through the hole, but in the fluid, system installed with the dip-coated Al plate, the pressure in the channel was lower than the infiltration pressure of the pressure barrier formed on the superhydrophobicity hole. In addition, in the fluid system where water and air flowed together, as shown in Figures 18(c) and (d), water flowing through the hole in the uncoated Al plate blocked the hole and trapped the air, but the hole on the dip-coated Al plate showed that air was vented through the hole. Additionally, the dip-coated Ni foam sheet also showed that water could not flow out due to pressure barrier as shown in Figure 19. Using these results, a pressure relief valve can be configured without installing a separate device and can be applied by adding small components as shown in Figure 20.

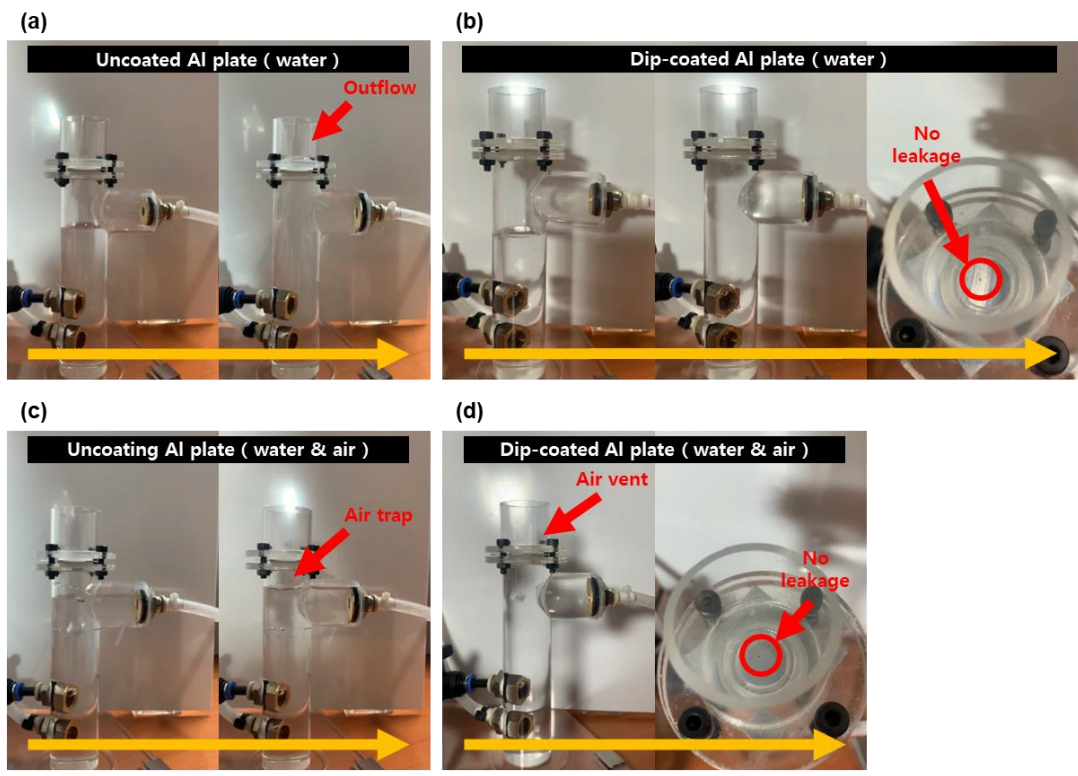Figure 18. Demonstration of a fluid channel with pressure barrier, (a) uncoated Al plate(water), (b) dip-coated Al plate(water), (c) uncoated Al plate (water and air), (d) dip-coated Al plate(water and air)
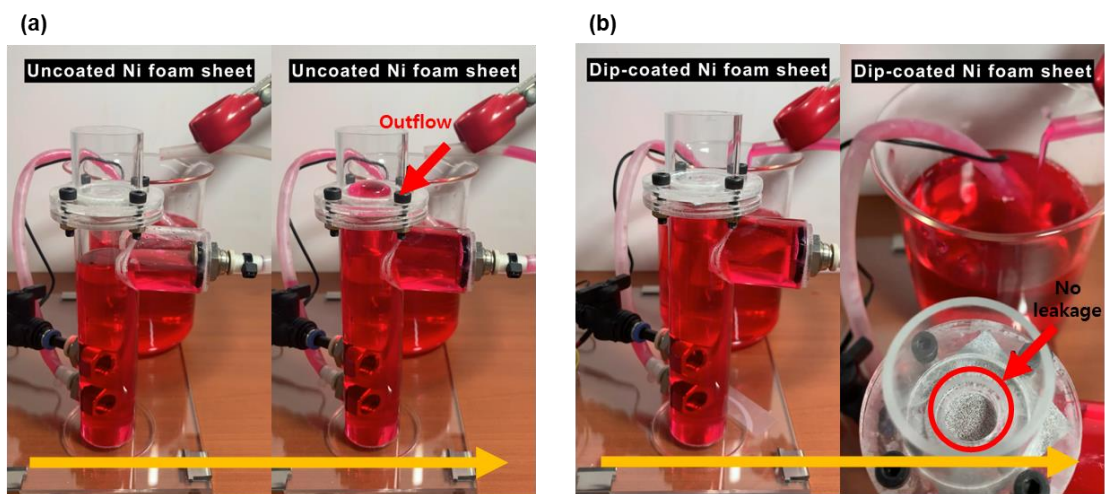

Figure 19. Demonstration of a fluid channel with pressure barrier, (a) uncoated Ni foam sheet(water), (b) dip-coated Ni foam sheet(water).
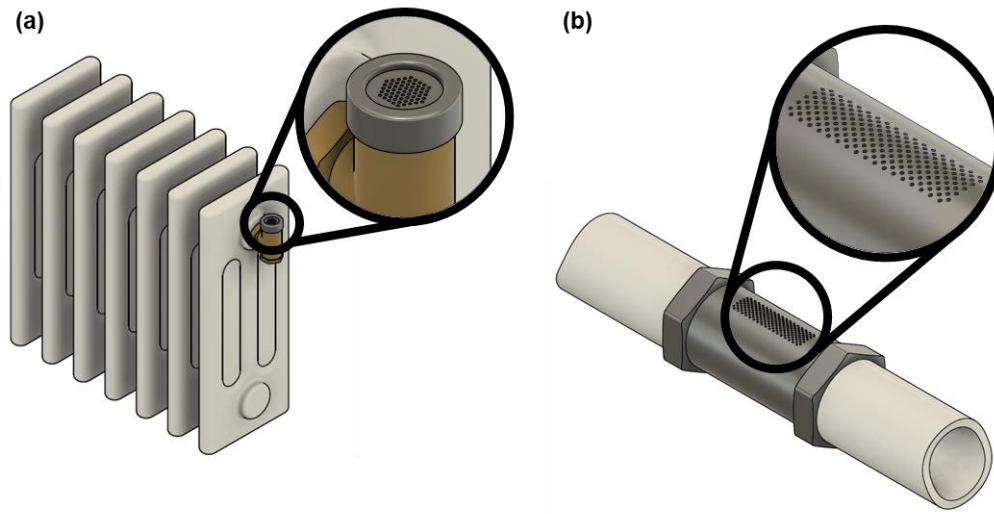
Figure 20. Application of pressure relief device, (a) cap type, (b) channel type.

4. CONCLUSIONS

In summary, a pressure barrier is formed interface of water and the surface by surface tension in a hole or channel that is superhydrophobicity. The infiltration pressure of the pressure barrier can be estimated according to Young-Laplace equation and is not affected by the number of holes. The degree of relief pressure varies depending on the direction of the hole axis, and in a direction consistent with gravity, the termination of the relief is predictable. In this study, the effect of pressure barrier on the holes of the superhydrophobic surface produced using the dip coating method, a simple fabrication method, was investigated. Despite the dip-coated surface that is not completely uniform, it demonstrated the feasibility that the infiltration pressure of the pressure barrier is formed according to Young-Laplace equation. In addition, experiments on the effects of pressure barrier on micro/nano scale hole and channel with uniform hydrophobic or superhydrophobic surfaces are expected. Furthermore, the results are expected to contribute to a novel type of pressure relief device.

REFERENCES

[1]   Mawatari, K., Kubota, S., Xu, Y., Priest, C., Sedev, R., Ralston, J., and Kitamori, T., 2012, "Femtoliter Droplet Handling in Nanofluidic Channels: A Laplace Nanovalve," Anal. Chem., **84**(24), pp. 10812–10816.

[2]   Wu, R., Kharaghani, A., and Tsotsas, E., 2016, "Two-Phase Flow with Capillary Valve Effect in Porous Media," Chem. Eng. Sci., **139**, pp. 241–248.

[3]   Leu, T. S., and Chang, P. Y., 2004, "Pressure Barrier of Capillary Stop Valves in Micro Sample Separators," Sensors Actuators, A Phys., **115**(2-3 SPEC. ISS.), pp. 508–515.

[4]   Londe, G., Chunder, A., Wesser, A., Zhai, L., and Cho, H. J., 2008, "Microfluidic Valves Based on Superhydrophobic Nanostructures and Switchable Thermosensitive Surface for Lab-on-a-Chip (LOC) Systems," Sensors Actuators, B Chem., **132**(2), pp. 431–438.

[5]   Takei, G., Nonogi, M., Hibara, A., Kitamori, T., and Kim, H. B., 2007, "Tuning Microchannel Wettability and Fabrication of Multiple-Step Laplace Valves," Lab Chip, **7**(5), pp. 596–602.

[6]   De Gennes, Pierre-Gilles, Françoise Brochard-Wyart, D. Q., 2013, *Capillarity and Wetting Phenomena: Drops, Bubbles, Pearls, Waves.*

[7]   Zheng, Q. S., Yu, Y., and Zhao, Z. H., 2005, "Effects of Hydraulic Pressure on the Stability and Transition of Wetting Modes of Superhydrophobic Surfaces," Langmuir, **21**(26), pp. 12207–12212.

[8]   Chang, H., Tu, K., Wang, X., and Liu, J., 2015, "Fabrication of Mechanically Durable Superhydrophobic Wood Surfaces Using Polydimethylsiloxane and Silica Nanoparticles," RSC Adv., **5**(39), pp. 30647–30653.

[9]   Roach, P., Shirtcliffe, N. J., and Newton, M. I., 2008, "Progess in Superhydrophobic Surface Development," Soft Matter, **4**(2), p. 224.

[10]   Lee, K. M., Park, H., Kim, J., and Chun, D. M., 2019, "Fabrication of a Superhydrophobic Surface Using a Fused Deposition Modeling (FDM) 3D Printer with Poly Lactic Acid (PLA) Filament and Dip Coating with Silica Nanoparticles," Appl. Surf. Sci., **467**–**468**(September 2018), pp. 979–991.

[11]   Chung, D. C. K., Huynh, S. H., Katariya, M., Chan, A. Y. C., Wang, S., Jiang, X., Muradoglu, M., Liew, O. W., and Ng, T. W., 2017, "Drops on a Superhydrophobic Hole Hanging on under Evaporation," ACS Omega, **2**(9), pp. 6211–6222.

[12]   Ganesh, V. A., Nair, A. S., Raut, H. K., Yuan Tan, T. T., He, C., Ramakrishna, S., and Xu, J., 2012, "Superhydrophobic Fluorinated POSS-PVDF-HFP Nanocomposite Coating on Glass by Electrospinning," J. Mater. Chem., **22**(35), pp. 18479–18485.

[13]   Han, H., and Kim, C., 2014, "Dispensing of Rheologically Complex Fluids at the Dripping Regime," J. Nonnewton. Fluid Mech., **213**, pp. 57–67.

[14]   Ibach, H., 2006, *Physics of Surfaces and Interfaces*.

[15]   Nikitas, P., and Pappa-Louisi, A., 1990, "Thermodynamic and Modelistic Study of Surface Solutions: Aqueous Solutions Containing 2-Butanol," J. Phys. Chem., **94**(1), pp. 361–370.

[16] Iglauer, S., Salamah, A., Sarmadivaleh, M., Liu, K., and Phan, C., 2014, "Contamination of Silica Surfaces: Impact on Water-CO2-Quartz and Glass Contact Angle Measurements," Int. J. Greenh. Gas Control, **22**, pp. 325–328.

[17] Eleshaky, M. E., 2017, "ICNMM2016-7992."

[18] Kazemzadeh, A., Ganesan, P., Ibrahim, F., He, S., and Madou, M. J., 2013, "The Effect of Contact Angles and Capillary Dimensions on the Burst Frequency of Super Hydrophilic and Hydrophilic Centrifugal Microfluidic Platforms, a CFD Study," PLoS One, **8**(9), pp. 1–12.